ACS Macro Letters

Letter

pubs.acs.org/macroletters

Assembly of Polymer-Tethered Gold Nanoparticles under Cylindrical Confinement

Ruijing Liang, Jiangping Xu, Renhua Deng, Ke Wang, Shanqin Liu, Jingyi Li, and Jintao Zhu*

Key Laboratory of Large-Format Battery Materials and System of Ministry of Education, School of Chemistry and Chemical Engineering, Huazhong University of Science and Technology, Wuhan 430074, China

Supporting Information

ABSTRACT: The assembly of polystyrene (PS)-tethered gold nanoparticles (Au@PS NPs) in anodic aluminum oxide (AAO) cylindrical nanopores was investigated. This cylindrical confined assembly strategy allows us to generate novel assemblies (e.g., linear chain, zigzag, two-NP layer, three-NP layer, and hexagonally packed NP structures) by manipulating the AAO membrane pore size and molecular weight of PS ligands. Moreover, the optical property of the hybrid assemblies can be tuned through varying the interparticle distances and assembly structures. This work provides a guideline for confined assembly of functional NPs and lays groundwork for fabricating well-ordered hybrid nanostructures for optical, electronic, biosensing, and data storage devices.

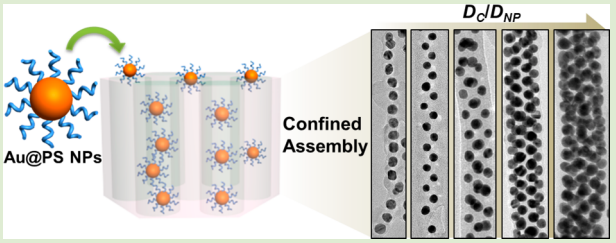

Controlled assembly of functional nanoparticles (NPs) into one-dimensional (1D),[1,2] 2D,[3] and 3D[4] hierarchical structures provides an effective route for the fabrication of advanced materials and devices with unique optical, electronic, and magnetic properties. Recently, supramolecular assemblies constructed by inorganic NPs were successfully achieved through directional chemical binding,[1] templating (e.g., boron nitride nanotube or carbon nanotube),[5−7] external force (e.g., electric or magnetic field),[8] and biomolecular recognition (e.g., DNA or peptide).[9,10] Among the building blocks for assembly, polymer-tethered NPs attract much attention due to their unique physical and chemical properties, which can improve the stability, designability, and functionality of the resulting assemblies. For example, Nie and co-workers used polystyrene (PS)-coated gold nanorods to construct multidimensional functional architectures.[11] Recently, Au NPs decorated with amphiphilic block copolymers (BCPs) or mixed polymer ligands were applied to fabricate plasmonic vesicles, which have valuable applications in bioimaging and cancer therapy.[12,13] Particularly, 1D assemblies are of great interest for a wide variety of applications in sensing, imaging, electronic devices, catalysis, and medical diagnostics owing to the unique localized surface plasmon resonance (LSPR) and large surface energy of the self-organized structures (e.g., tunable plasmonic wavelength and coupling effect).[14,15] However, it is difficult to fabricate 1D assemblies with novel structures, like zigzag, single- or double-helices, and two-NP layer, by assembling the hybrid NPs through conventional approaches. Thus, it still remains a big challenge to effectively produce the hybrid assemblies with hierarchical structures.

Confined assembly has attracted much attention due to its ability to break the symmetry of a structure, thus allowing for the formation of novel structures which are not available in bulk.[16−22] Cylindrical nanochannels, as observed in porous anodic aluminum oxide (AAO), provide a desirable space for 2D confined assembly. Great progress has been achieved in controlled assembly of BCPs into a variety of novel nanostructures in cylindrical nanopores, demonstrating that 2D confinement provides a powerful route to produce nanomaterials with unique structures and properties.[16−23] Also, spherical BCP micelles, acting as soft building blocks, were introduced into the AAO nanochannels, and novel aggregates (e.g., linear chain, zigzag, and double-helical structures) were obtained.[24] In this case, the micelles could adjust their size and morphology in the confined space owing to the soft nature of the micelles. By contrast, hard spheres with larger size (e.g., silica or cross-linked PS NPs) could be infiltrated into confined channels to form colloidal crystal wires.[25−27] The formed structures can be further fixed by introducing a silica shell encased outside[25] or infiltrating the inorganic or organic precursors in the nanochannels.[26,27] Generally, size and shape of the hard NPs are difficult to be adjusted, and thus wide confined channels were usually employed. Yet, novel hierarchical structures (e.g., zigzag, single- or double-helical, and two-NP layer structures) could not be conveniently obtained due to the weakened confinement of the quite wide channels, limiting the functionality and further applications of the assemblies. It is thus highly desirable to fabricate metal NP assemblies with tunable interparticle distance, various internal structures, and advanced functions in a simple and efficient way.

Here, we report the 2D confined assembly of PS-tethered Au NPs (named as Au@PS NPs) in AAO cylindrical nanochannels

Received: April 9, 2014
Accepted: May 6, 2014
Published: May 8, 2014

 © 2014 American Chemical Society dx.doi.org/10.1021/mz5002146 | ACS Macro Lett. 2014, 3, 486−490

(see Figure 1 and Figure S1, Supporting Information). Such polymer-coated Au NPs are the combination of a soft polymer

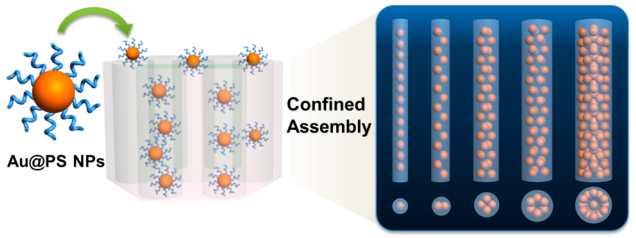

Figure 1. Illustration showing the strategy for confined assembly of polymer-tethered NPs in cylindrical nanopores to fabricate the hybrid assemblies with different inner structures, e.g., linear chain, zigzag, two-NP layer, three-NP layer, and hexagonally packed structures depending on the 2D confined effect.

shell and a hard metal NP core. Supramolecular assemblies with various novel nanostructures, such as linear chain, zigzag, two-NP layer, three-NP layer, and hexagonally packed NP structures, can be obtained by varying the size of the nanochannels and/or molecular weight of the tethered polymers. Our results demonstrate that the confined effect exhibits a significant influence on not only the stretching of the polymer chains but also the packing style of the metal NPs.[24] Furthermore, this strategy shows the advantages that polymer brushes on the metal NPs make the assemblies more stable (Figure S1d, Supporting Information) and help the formation of novel assemblies by adjusting their chain stretching within the confined space, while the metal NPs endow hybrid assemblies with functionality, broadening their applications in biosensing, optical device, and data storage.

In a typical experiment, monodispersed Au NPs (size: 16.0 ± 1.1 nm) coated with sodium citrate were prepared using a previously reported citrate reduction approach, while Au@PS NPs were obtained through the ligand exchange route (see the Supporting Information for experimental details).[28] Then, Au@PS NPs were dispersed in chloroform (~3 mg·mL^{-1}), and the AAO membrane was immersed in the NP dispersion. As the solvent evaporated, Au@PS NPs entered the cylindrical nanopores due to the capillary force and the attractive interaction between the AAO membrane and the NP solution and organized into supramolecular assemblies with various structures (Figure S1b–d, Supporting Information). The individual hybrid assemblies were obtained through complete solvent evaporation and removal of the AAO template by sodium hydroxide aqueous solution.

When confined in 2D cylindrical space, hard spherical particles (e.g., silica NPs) can pack in a minimum-energy configuration and form different assemblies by varying D_C/D_S, where D_C and D_S are the diameter of the channel and the spherical particles, respectively.[25−27,29] In this study, we define the pore size of the membrane and overall diameter of Au@PS NPs as D_C and D_{NP}, respectively. We thus can tune D_C/D_{NP} from a different combination of various pore sizes of the AAO membrane (e.g., 18.8, 61.8, 96.3, and 210.2 nm, see Table 1) and Au@PS NPs with different PS molecular weight (M_n, e.g., 5k, 11.5k, 29k, and 50k). The overall diameter of PS-tethered Au NPs including the Au core plus the PS shell of Au@PS$_{5k}$, Au@PS$_{11.5k}$, Au@PS$_{29k}$, and Au@PS$_{50k}$ is, respectively, 18.7 ± 1.1 nm, 20.1 ± 1.4 nm, 25.3 ± 2.0 nm, and 31.4 ± 2.0 nm, which was estimated from TEM results (Table 1 and Figure S2, Supporting Information), assuming that the PS shell is a solid layer on the surface of Au NPs. Both D_C and D_{NP} will affect the interparticle distance and the resulting structure of assemblies, which provide new dimensionality to control the optical properties of the assemblies and apply in sensors, nonlinear optics, and catalysis.[30,31]

Figure 2 displayed the representative hybrid assemblies with different interesting structures by introducing the Au@PS NPs into the cylindrical nanopores. The inner structure and morphology of the hybrid assemblies can be tuned by manipulating the AAO membrane pore size and molecular weight of the PS ligands. When the confined space is very narrow (e.g., 18.8 nm, Figure 2a–d), the D_C/D_{NP} presents the lower value of 0.60 to 1.01 (Table 1). Surprisingly, Au@PS NPs with overall size larger than that of the nanochannels could also enter the channels and form linear chain-like assemblies. Presumably, polymer brushes on the surface of Au NPs could adjust their chain stretching to make the NPs enter the nanochannels. The confined effect of the nanochannel will further compress the polymer chain along the horizontal direction of the nanochannel, leading to the decrease of the apparent size of Au@PS NPs. As a consequence, a Au@PS NP consisting of a hard metal core and a soft polymer shell could enter the channel whose diameter was smaller than that of the overall NP. This interesting behavior cannot be observed for hard particles when $D_C/D_{NP} < 1$ due to the incompressibility of the particles.[29] More interestingly, the stretching degree of the polymer chains will vary with the variation of the molecular weight of the polymers, hence altering the interparticle distance in the hybrid assemblies (Figure 3a). For the polymer chains with high molecular weight (e.g., 29k and 50k), the polymer chain was highly stretched due to the lower grafting density

Table 1. Characteristic of Au NPs Employed in This Study and D_C/D_{NP}

Au NPs		Au@citrate	Au@PS$_{5k}$	Au@PS$_{11.5k}$	Au@PS$_{29k}$	Au@PS$_{50k}$
D_{NP}[a] (nm)		16.0	18.7	20.1	25.3	31.4
w_{PS}[b] (wt %)		—	29.96%	29.80%	34.10%	35.80%
Σ[c] (chains/nm^2)		—	2.65	1.14	0.55	0.35
D_C[d]/D_{NP}	D_C (nm)					
	18.8	1.17	1.01	0.94	0.74	0.60
	61.2	3.82	3.27	3.04	2.42	1.95
	96.3	6.01	5.15	4.79	3.81	3.07
	210.2	13.11	11.24	10.46	8.31	6.69

[a] D_{NP} refers to the overall diameter of the Au NP obtained by calculating about 100 samples in TEM images. [b] w_{PS} denotes the weight ratio of the tethered PS to total Au@PS NPs obtained by TGA. [c] Σ presents the grafting density of PS on Au NPs. [d] D_C represents the average pore size of the AAO membrane determined by SEM images.

dx.doi.org/10.1021/mz5002146 | ACS Macro Lett. 2014, 3, 486−490

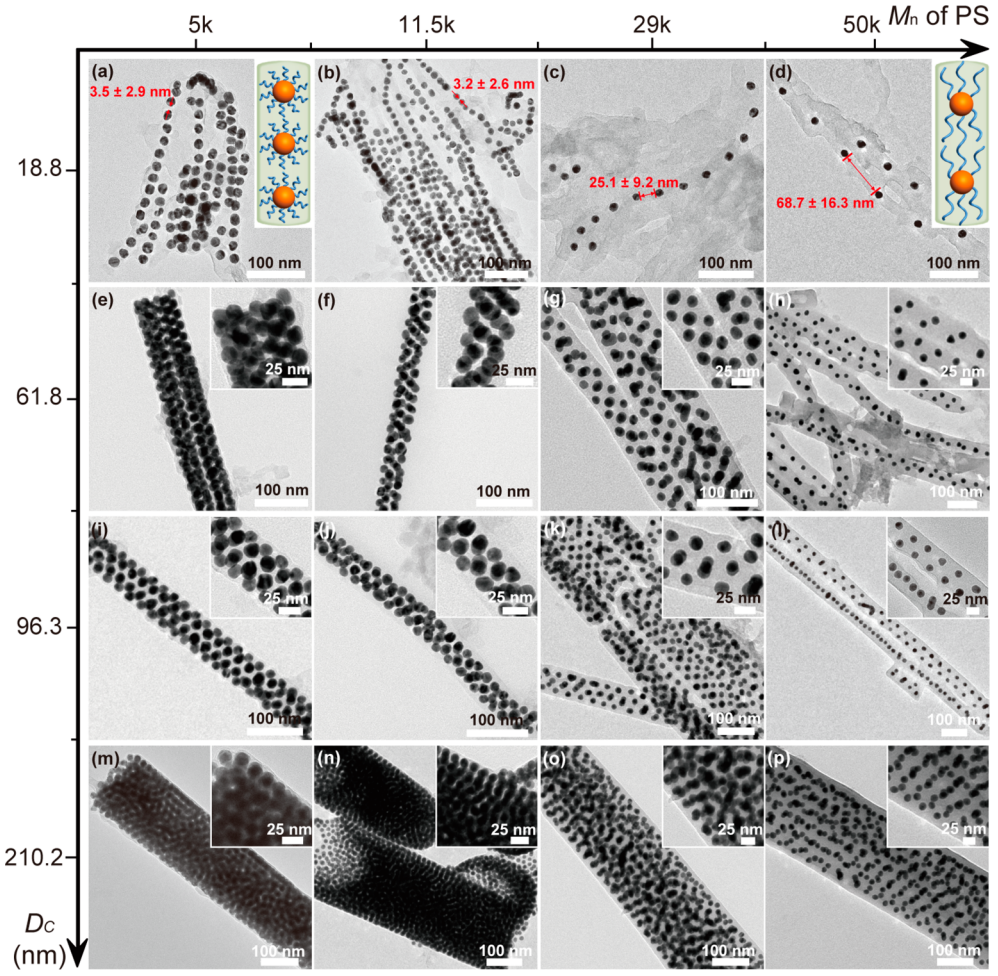

Figure 2. Representative TEM images of the hybrid assemblies with various structures by adjusting the AAO membrane pore size and PS molecular weight. The images display Au@PS_{5k}, Au@$PS_{11.5k}$, Au@PS_{29k}, and Au@PS_{50k} in AAO channels with pore size of 18.8 nm (a)−(d), 61.8 nm (e)−(h), 96.3 nm (i)−(l), and 210.2 nm (m)−(p), respectively. Insets in the upper right of (a) and (d) are the schematic illustration of the PS chain stretching in the confined space. Insets in the upper right of (e)−(p) are the magnified TEM images of the corresponding hybrid assemblies.

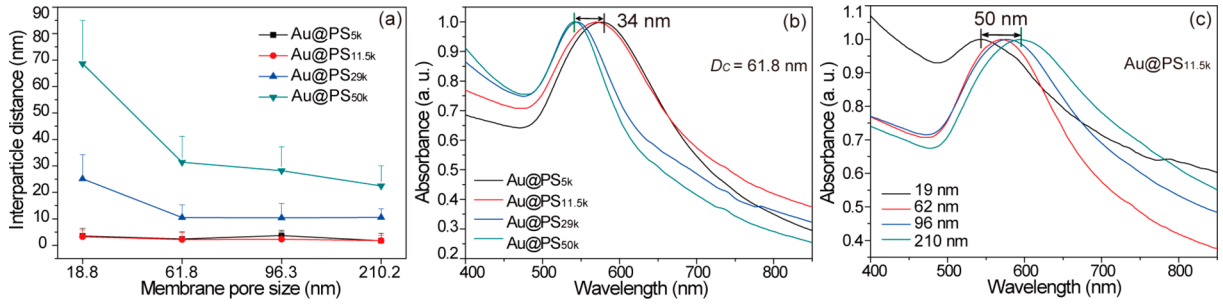

Figure 3. (a) Plot showing the relationship between the interparticle distances of various assemblies in different membrane pore sizes. All the data are obtained by calculating about 100 samples from TEM images. Error bars represent the standard deviation. (b) UV−vis spectra of different assemblies organized from different kinds of Au@PS NPs confined in 61.8 nm AAO membranes, respectively. (c) UV−vis spectra of different assemblies organized from Au@$PS_{11.5k}$ confined in the AAO membranes with various pore sizes, respectively.

(0.55 and 0.35 chain/nm^2, respectively) and higher stretching ability (inset in Figure 2d). Thus, the interparticle distance greatly increases from 3.5 nm (Figure 2a, PS_{5k}) to 25.1 nm (Figure 2c, PS_{29k}) and to 68.7 nm (Figure 2d, PS_{50k}). By contrast, for Au@PS_{5k} and Au@$PS_{11.5k}$, as the chain length is much less than that of Au@PS_{29k} and Au@PS_{50k}, the PS chains are less flexible, while the grafting density of the polymer chains is high (2.65 and 1.14 chain/nm^2, respectively). Although the PS chains are also forced to stretch along the horizontal direction of the nanochannel due to the confined effect, the stretching degree is not as large as that of Au@PS_{29k} and Au@PS_{50k}. As a result, the stretching of the PS chains on Au@PS_{5k} and Au@$PS_{11.5k}$ is quite insignificant to increase the interparticle distance (3.5 and 3.2 nm, respectively, Figure 2a,b). In this case, these two kinds of hybrid NPs behave more like hard spheres.

Raising the AAO membrane pore size will increase D_C/D_{NP} and hence weaken the confined effect on the assembly. For

dx.doi.org/10.1021/mz5002146 | ACS Macro Lett. 2014, 3, 486−490

example, when the pore size is 61.8 nm, novel assemblies with two-NP layer structures from Au@PS_{5k}, Au@$PS_{11.5k}$, and Au@PS_{29k} NPs were obtained (Figure 2e−g). Similarly, the interparticle distance in two-NP layer structures increases with the increase of the PS brush molecular weight (Figure 3a). Particularly, when Au@PS_{50k} NPs were inserted into the nanochannel with pore size of 61.8 nm, zigzag structure (Figure 2h) was obtained to retain the minimum-energy and maximum filling fraction, showing a decrease of the interparticle distance (Figure 3a).

When the pore size reaches 96.3 nm, the confined effect is more weakened. In this case, a three-NP layer structure was observed from the assembly of Au@PS_{5k} and Au@$PS_{11.5k}$ (Figure 2i,j). As mentioned above, PS brushes with high molecular weight (PS_{29k} and PS_{50k}) give rise to a more flexible molecular conformation change in the confined space (Figure 2k,l). Interestingly, the assemblies still keep almost the same inner structure and interparticle distance as that in the 61.8 nm confined space (Figures 2g,h and 3a). Further increasing the nanopore size to 210.2 nm (much larger than that of Au@PS NPs) induces the NPs to stack largely in a conventional bulk-crystal stacking manner and produce the hexagonally packed structures (Figure 2m−p) since the boundary conditions imposed by the cylindrical walls become quite insignificant. This can be confirmed by the result that the interparticle distance of Au@PS NPs in 210.2 nm confined space (Figure 3a) is only slightly smaller than that in the monolayer packing film (seen as the bulk stacking, Figure S2, Supporting Information). In this case, the overall size of Au@PS NP plays an apparent role in tuning the interparticle spacing.

The above results indicate that the confined effect has a great influence on the morphology and inner structure of the hybrid assemblies. As the molecular weight of the tethered polymers increases and confined space decreases, the confined effect is enhanced. Similar to the theoretical results of BCP[16,17,32] or hard spheres[29] under 2D cylindrical confinement, the value of D_C/D_{NP} is one of the most important factors which determines the polymer-tethered NP packing types of the resulting assemblies and the interparticle distance between the NPs. When D_C/D_{NP} is small and noninteger, a strong confined effect is exerted on the building blocks. Thus, it will show apparent frustration, and the assemblies with novel structures emerge. When the pore size is 18.8 nm (D_C/D_{NP} ranged from 0.60 to 1.01, Table 1), the cylindrical nanochannel presents the strongest confined effect, leading to the linear chain structure of the assemblies (Figure 2a−d). By contrast, when D_C/D_{NP} rises from 6.69 to 11.24 in 210.2 nm channels, an insignificant confined effect is exerted on the Au@PS NPs. Thus, the assemblies keep the bulk-crystal stacking morphology (Figure 2m−p). As the pore sizes range from 18.8 to 210.2 nm, D_C/D_{NP} values are relatively small and noninteger. Hence, the cylindrical nanochannels exert effective confined effect on the NPs and induce the frustration of the building blocks. Novel structures (e.g., zigzag structure, two-NP layer, and three-NP layer) can be obtained by tuning the pore size of the nanochannels and/or the molecular weight of the tethered polymers.

This strategy allows us to tune the internal structures of the NP ensemble and the interparticle distance which will greatly influence the optical property of the hybrid assemblies (i.e., the plasma resonance absorption peak). The SPR absorption of the hybrid assemblies is shown in Figure 3b,c and Figure S3 (Supporting Information). Taking the AAO membrane with pore size of 61.8 nm, for example, the interparticle spacing increases with the increase of the molecular weight of tethered PS, leading to a 34 nm blue-shift of SPR due to the plasmon coupling (Figure 3b). Moreover, when Au@$PS_{11.5k}$ is confined in the AAO membrane with different pore sizes, hybrid assemblies with various internal structures were observed, which also apparently influence the SPR. In this case, a 50 nm red-shift of SPR was observed from the well-ordered packing of a large amount of Au@$PS_{11.5k}$ NPs (Figure 3c).

In summary, we demonstrated a facile and efficient route to prepare the hierarchical polymer-tethered Au NP assemblies with novel and stable morphologies under 2D cylindrical confinement. The results indicated that the confined effect (D_C/D_{NP}) played a key role in determining the morphology of the hybrid assemblies. Structures as well as the interparticle distance of the Au NPs in the assemblies can be readily tailored by varying the confined space and molecular weight of the tethered polymers. The optical property of the hybrid assemblies can also be tuned through varying the structures and interparticle spacing of assemblies. These hybrid assemblies with well-ordered structures and advanced functions will find potential applications in sensor, catalysis, data storage, and biomedicine.

■ ASSOCIATED CONTENT

Supporting Information

Experimental details, SEM images of the hybrid NP assemblies in AAO channels, TEM images of monolayer packing of NPs, and UV−vis spectra of the hybrid assemblies. This material is available free of charge via the Internet at http://pubs.acs.org.

■ AUTHOR INFORMATION

Corresponding Author

*E-mail: jtzhu@mail.hust.edu.cn.

Notes

The authors declare no competing financial interest.

■ ACKNOWLEDGMENTS

We gratefully acknowledge funding for this work provided by the National Basic Research Program of China (973 Program, 2012CB821500), National Natural Science Foundation of China (91127046), and Excellent Youth Foundation of Hubei Scientific Committee (2012FFA008). We also thank the HUST Analytical and Testing Center for allowing us to use its facilities.

■ REFERENCES

(1) DeVries, G. A.; Brunnbauer, M.; Hu, Y.; Jackson, A. M.; Long, B.; Neltner, B. T.; Uzun, O.; Wunsch, B. H.; Stellacci, F. *Science* **2007**, *315*, 358−361.

(2) Li, W.; Zhang, P.; Dai, M.; He, J.; Babu, T.; Xu, Y.-L.; Deng, R.; Liang, R.; Lu, M.-H.; Nie, Z.; Zhu, J. *Macromolecules* **2013**, *46*, 2241−2248.

(3) Tang, Z.; Zhang, Z.; Wang, Y.; Glotzer, S. C.; Kotov, N. A. *Science* **2006**, *314*, 274−278.

(4) Macfarlane, R. J.; Lee, B.; Jones, M. R.; Harris, N.; Schatz, G. C.; Mirkin, C. A. *Science* **2011**, *334*, 204−208.

(5) Mickelson, W.; Aloni, S.; Han, W.-Q.; Cumings, J.; Zettl, A. *Science* **2003**, *300*, 467−469.

(6) Khlobystov, A. N.; Britz, D. A.; Ardavan, A.; Briggs, G. A. D. *Phys. Rev. Lett.* **2004**, *92*, 245507.

(7) Correa-Duarte, M. A.; Pérez-Juste, J.; Sánchez-Iglesias, A.; Giersig, M.; Liz-Marzán, L. M. *Angew. Chem., Int. Ed.* **2005**, *44*, 4375−4378.

(8) Leunissen, M. E.; Vutukuri, H. R.; van Blaaderen, A. *Adv. Mater.* **2009**, *21*, 3116−3120.
(9) Sharma, J.; Chhabra, R.; Cheng, A.; Brownell, J.; Liu, Y.; Yan, H. *Science* **2009**, *323*, 112−116.
(10) Chen, C.-L.; Zhang, P.; Rosi, N. L. *J. Am. Chem. Soc.* **2008**, *130*, 13555−13557.
(11) Nie, Z.; Fava, D.; Kumacheva, E.; Zou, S.; Walker, G. C.; Rubinstein, M. *Nat. Mater.* **2007**, *6*, 609−614.
(12) He, J.; Liu, Y.; Babu, T.; Wei, Z.; Nie, Z. *J. Am. Chem. Soc.* **2012**, *134*, 11342−11345.
(13) Song, J.; Zhou, J.; Duan, H. *J. Am. Chem. Soc.* **2012**, *134*, 13458−13469.
(14) Gong, J.; Li, G.; Tang, Z. *Nano Today* **2012**, *7*, 564−585.
(15) Nakao, H. *Anal. Sci.* **2014**, *30*, 151−156.
(16) Chen, P.; He, X.; Liang, H. *J. Chem. Phys.* **2006**, *124*, 104906.
(17) Shi, A.-C.; Li, B. *Soft Matter* **2013**, *9*, 1398−1413.
(18) Shin, K.; Xiang, H.; Moon, S. I.; Kim, T.; McCarthy, T. J.; Russell, T. P. *Science* **2004**, *306*, 76.
(19) Ma, M.; Titievsky, K.; Thomas, E. L.; Rutledge, G. C. *Nano Lett.* **2009**, *9*, 1678−1683.
(20) Chen, D.; Park, S.; Chen, J.-T.; Redston, E.; Russell, T. P. *ACS Nano* **2009**, *3*, 2827−2833.
(21) Lee, C.-W.; Wei, T.-H.; Chang, C.-W.; Chen, J.-T. *Macromol. Rapid Commun.* **2012**, *33*, 1381−1387.
(22) Mei, S.; Wang, L.; Feng, X.; Jin, Z. *Langmuir* **2013**, *29*, 4640−4646.
(23) Wang, Y.; Tong, L.; Steinhart, M. *ACS Nano* **2011**, *3*, 1928−1938.
(24) Thomas, A.; Schierhorn, M.; Wu, Y.; Stucky, G. *J. Mater. Chem.* **2007**, *17*, 4558−4562.
(25) Li, F.; Badel, X.; Linnros, J.; Wiley, J. B. *J. Am. Chem. Soc.* **2005**, *127*, 3268−3269.
(26) Li, F.; He, J.; Zhou, W. L.; Wiley, J. B. *J. Am. Chem. Soc.* **2003**, *125*, 16166−16167.
(27) Moon, J. H.; Kim, S.; Yi, G.-R.; Lee, Y.-H.; Yang, S.-M. *Langmuir* **2004**, *20*, 2033−2035.
(28) Li, W.; Liu, S.; Deng, R.; Zhu, J. *Angew. Chem., Int. Ed.* **2011**, *50*, 5865−5868.
(29) Pickett, G. T.; Gross, M.; Okuyama, H. *Phys. Rev. Lett.* **2000**, *85*, 3652−3655.
(30) Cong, V. T.; Ganbold, E.-O.; Saha, J. K.; Jang, J.; Min, J.; Choo, J.; Kim, S.; Song, N. W.; Son, S. J.; Lee, S. B.; Joo, S. W. *J. Am. Chem. Soc.* **2014**, *136*, 3833−3841.
(31) Ghosh, S. K.; Pal, T. *Chem. Rev.* **2007**, *107*, 4797−4862.
(32) Dobriyal, P.; Xiang, H.; Kazuyuki, M.; Chen, J.-T.; Jinnai, H.; Russell, T. P. *Macromolecules* **2009**, *42*, 9082−9088.